Materials Advances

ROYAL SOCIETY OF CHEMISTRY

PAPER

View Article Online
View Journal | View Issue

Cite this: *Mater. Adv.*, 2025, **6**, 7906

Self-assembly of carbamylated lysine repeat peptide amphiphiles into fibrillar nanostructures

Vivek Shekhar, †[a] Tamalika Paul, †[b] Joshna Gadhavi *[c] and Sharad Gupta *[a]

Peptide amphiphilicity enables self-assembly, forming well-defined structures such as micelles and polymersomes. The exploration of hydrophilic lysine-rich peptides with hydrophobic lipid modifications at the N-terminus to form self-assembling peptide amphiphiles as a strategy is explored in this study. Carbamylation, a post-translational modification known to promote the aggregation of proteins, reported in neurodegenerative disorders, is exploited for charge neutralization of lysine residues, thereby inducing amyloidogenicity in peptides. In our study, we synthesized a series of lysine repeat peptides (3K, 5K, and 8K) of variable lengths with a combination of hydrophobic tailing (C2, C6, and C9) as models using SPPS (solid-phase peptide synthesis). The amyloidogenic properties of carbamylated lysine peptides, including aggregation kinetics, were studied through several assays to assess the structural and functional implications of carbamylation on self-assembling peptide amphiphiles. We also compared the morphological similarities and differences using microscopic imaging techniques, such as bright-field, fluorescence, and scanning electron microscopy, to visualize and characterize the fibrillar assembly across these model peptides. The synthesized self-assembling amphiphiles can be tuned for use in various applications, including drug delivery carrier development, tissue engineering, antifouling, antifogging, and dye degradation modality.

Received 13th December 2024,
Accepted 8th September 2025

DOI: 10.1039/d4ma01239a

rsc.li/materials-advances

Introduction

Peptide amphiphiles share the physicochemical and structural features of amphiphilic surfactants, including intrinsic self-assembly properties that lead to diverse nanostructures. The very nature of these lipopeptides, which contain a hydrophilic peptide sequence with a hydrophobic lipid tail, allows for the self-assembly of these amphiphiles.[1] The hydrophobic interactions from the alkyl chains at the N-terminus and the attractive forces among the backbones and side chains of peptides play a crucial role in the assembly. Both the hydrophilic residues of the peptide and the hydrophobic alkyl chain lengths can be modified and tuned to develop desired nanostructures. Certain amino acids, such as lysine, arginine, and histidine, can be used to synthesize peptide amphiphiles, which can also act as surfactants.[2] Over the years, the utility of designer peptide amphiphiles has been explored extensively in fields such as chemistry, materials science, and biology due to their tailoring efficiency and versatility, especially for targeted applications.[3]

Depending on the nature of the monomers and the nanostructures produced, the mechanism driving their self-assembly tends to vary intriguingly, with significant differences in hydrogen bonding, van der Waals forces, π–π stacking, hydrophobic interactions, and anion–π or cation–π interactions among the several known non-covalent interactions.[4] The widely known example of an amphiphilic assembly enabling compartmentalization in biology is through the plasma membrane, where a balance in the number and variation of the entities that contribute towards achieving the optimal hydrophilic–lipophilic balance remains essential to offer such distinct functionality.[5] Introducing minor alterations to this balance can provide for a range of nanostructures with differences in properties in the order of magnitude, leading to an attractive prospect to study the kinetics of such phenomena.[6]

Self-assembly of peptide amphiphiles can give rise to bilayer, micellar, and nanofibrillar structures.[7,8] Peptide-amphiphile-based supramolecular structures have been previously used to prepare hydrogels[9] with antibacterial activity.[10] Peptide-amphiphiles offer significant advantages due to their varied size, stiffness, and rheological (thixotropic) properties.[11] Amyloidogenicity of these self-assembling peptide amphiphiles can be harnessed for applications such as tissue engineering with

[a] *Department of Biological Sciences and Engineering, Indian Institute of Technology Gandhinagar, Gandhinagar, Gujarat, India. E-mail: sharad@iitgn.ac.in*
[b] *Department of Biomedical Sciences and Pathobiology, Virginia-Maryland College of Veterinary Medicine, Virginia Tech, Virginia, USA*
[c] *Department of Biochemistry, School of Medicine, Emory University, Atlanta, GA, USA. E-mail: joshna.gadhavi@emory.edu*
† Equal contribution.

2D and 3D cell culture scaffold alternatives,[12,13] target site drug delivery carriers, and controlled drug delivery systems,[14,15] and surfactant-like properties of these peptides for dye degradation,[16] while being both environmentally friendly and pollution-free with its organic and biocompatible approach.

Peptide amphiphile-based dynamic scaffolds, in particular, are designed to mimic native extracellular matrix properties, which can assist in cell proliferation, growth, and differentiation, along with crucial roles in performing complex cell-regulating activities like responses accounting for growth factor delivery, presentation of epitope, and changes to the environment with specific stimuli, such as light and enzymes.[17–19] The role of self-assembled peptide amphiphiles in regenerative medicine and stem cell research is poised to improve the catalog of biomaterial scaffold candidates that could help avoid the ethical concerns pertaining to induced pluripotent stem cells while not compromising on the reprogramming and regenerative capacity of the cells during the process.[20,21] Peptide amphiphiles, through self-assembly, seemingly show potential in providing a strategy to enable complex scaffold designs with their hierarchical structures found to resemble collagen with a nanofiber network leading to bundle development, creating fibers of micron-scales.[22–24]

Amyloidogenicity refers to the propensity of a protein (or peptides) to exhibit β-sheet structures in both parallel and anti-parallel conformations with a characteristic cross-linking pattern.[25] Amyloids tend to be filamentous, with sizes ranging from micro to nanoscale.[26] Typically, amyloids are observed in detrimental conditions such as Alzheimer's disease and other progressive neurodegenerative disorders. However, due to their structural capabilities and intrinsic properties, amyloids can also be harnessed across various functional applications.[27] One of these properties is the ability to self-assemble into defined structures. This niche of self-assembled amyloid structures offers improved mechanical resistance, chemical and thermal stability, biocompatibility, and enzymatic stability as opposed to the other classes of nanostructures.[28]

Carbamylation, a well-documented post-translational modification reaction, results in the addition of a covalent carbamoyl (–$CONH_2$) group, which can occur at either the N-terminus or at the ε-amino group of lysine, contributing towards the development of amyloid-like structures. In the presence of isocyanic acid, lysine residues have been found to undergo a non-enzymatic reaction in carbamylation, leading to carbamoyl modification, more commonly observed in renal and neurodegenerative disorders. In addition to lysine, side chains of several other amino acids, including cysteine, histidine, tyrosine, glutamic acid, and aspartic acid, have been proposed as potential targets for carbamylation by cyanates based on *in vitro* mechanistic studies.[29–32] However, the reaction appears to be much slower and is likely to yield less stable products compared to lysine. Elevated levels of carbamylated proteins have been reported in pathological conditions, such as chronic kidney disease (CKD), atherosclerosis, cardiovascular diseases (CVD) and certain brain disorders. Definitive *in vivo* evidence for the carbamylation of amino acids other than lysine remains lacking.[33–36] Under *in vitro* conditions, carbamylation is readily achieved with potassium cyanate (KCNO), involving incubation of proteins or peptides in an aqueous buffered condition at 37 °C.

Given the extreme stickiness of carbamylated lysines, to arrive at the carbamylation-supporting peptide amphiphiles, polylysine (lysine repeats 3K, 5K, 8K) peptides can be used as a surrogate to achieve efficient synthesis on a solid phase. At the same time, N-terminal modification with the introduction of alkyl chains of various lengths (C2, C6, C9) can offer a range of hydrophobicity in these amphiphiles. The ε-amine group of lysine can undergo a carbamylation reaction *in situ*, providing a charge neutralization effect and imparting amyloidogenicity in these peptides, enabling the polylysines to form self-assembled structures that otherwise do not occur.[37,38]

Our study provides an account of the aggregation kinetics and behavior of carbamylated lysine polypeptides with N-terminal modifications aimed at understanding the amyloidogenicity in peptide amphiphiles for harnessing their potential for forming self-assembled structures for various biomaterial applications.[39]

Experimental

General

The Fmoc-protected amino acids and all other chemical reagents, including thioflavin-T (ThT), were procured from Sigma-Aldrich, Iris Biotech, and Tokyo Chemical Industry Ltd (TCI) for this study. Molecular biology grade solutions and salts for the preparation of buffers were procured from Sisco Research Laboratories Ltd (SRL) Chemicals.

Synthesis of lysine repeat peptides with N-terminal modification

The polylysine peptides (3K, 5K, 8K) were synthesized manually by solid-phase peptide synthesis (SPPS) with Fmoc-based chemistry on a rink amide aminomethyl polystyrene resin (loading capacity of 0.64 mmol g^{-1}) with *N*,*N*′-diisopropylcarbodiimide-ethyl cyanohydroxyiminoacetate (DIC-Oxyma) as coupling agent and 1,8-diazabicyclo[5.4.0]undec-7-ene (DBU) -piperazine as Fmoc-deprotection solution using an in-house peptide synthesis set-up.[40] The N-terminal modifications were achieved using acetic anhydride-triethylamine (TEA) for the installation of the C2 tail and hexanoic acid and nonanoic acids (*via* DIC-oxyma activation) for the addition of C6 and C9 groups, respectively. The peptides were cleaved using a high-acid cleavage cocktail (95% trifluoroacetic acid (TFA), 2.5% triisopropyl silane (TIS), and 2.5% water) and precipitated with ice-cold diethyl ether. A combination of nine peptides (3KC2, 3KC6, 3KC9, 5KC2, 5KC6, 5KC9, 8KC2, 8KC6, and 8KC9) were synthesized. Homocitrulline variants of the 5K series of peptides, namely 5HCTC2, 5HCTC6 and 5HCTC9 (5HCT series) were synthesized using a microwave-assisted peptide synthesizer. The peptides were lyophilized, quantified, and stored at −80 °C until further experiments. The synthesized peptides were characterized by

matrix-assisted laser desorption/ionization-mass spectrometry (MALDI-MS) (Bruker Autoflex).

In situ carbamylation and the real-time aggregation kinetics of peptides by thioflavin-T (ThT) fluorescence assay

The synthesized peptides, both polylysines (3K, 5K and 8K series) and homocitrullines (5HCT series), before aggregation assay were monomerized with a hexafluoroisopropanol : trifluoroacetic acid (HFIP : TFA) (1 : 1) treatment overnight to break down preformed aggregates, if any. The mixture was evaporated with nitrogen gas to arrive at a thin residual film, which was then solubilized in ddH_2O. Various concentrations of the peptides (2.0, 1.0, 0.50, 0.25, 0.13, 0.06, 0.03 mg mL^{-1}) were subjected to aggregation assay in the presence of thioflavin-T (ThT) reporter dye (20 μM), which is known to bind selectively to fibrillar aggregates possessing β-sheet structures. For *in situ* carbamylation, 0.2 M KCNO was used as the polymerizing (carbamylating) agent,[37] and the aggregation kinetics was studied for all peptides at 37 °C using a multimode plate reader with excitation and emission at 450 nm and 485 nm, respectively. Brinkley Renaturing Buffer 80 (BRB80) (80 mM PIPES, 1 mM EDTA, and 1 mM $MgCl_2$) buffer at pH 6.8 was used for all aggregation assays. Readings were measured at 15-minute intervals with double orbital shaking for 30 seconds before every read. The process was monitored until the plateau (steady-state phase) fluorescence was reached (typically 3 days). The experiments were independently repeated at least three times, and the experimental replicates (pentaplicate) were averaged, after which the graphs were plotted using GraphPad Prism 9. The error bar represents the standard error.

Peptide characterization post carbamylation and aggregation with LC-MS

Post the aggregation assay, the aggregates were collected by ultra-centrifugation at 100 000 RCF at 4 °C to remove buffer salts. After washing with water, the samples were dried and subjected to a HFIP : TFA (1 : 1) monomerization treatment overnight. After obtaining a thin film of all nine peptides in monomeric form, they were solubilized in acetonitrile : water (50 : 50) and analyzed using liquid chromatography-mass spectrometry (LC-MS) (LCQ Fleet Ion Trap, Thermo Scientific) in ESI mode. The UPLC system was equipped with a reverse-phase C_{18} column (Supelco, 150 × 2.1 mm, 3.0 μm particle size, Sigma-Aldrich). Peptides were eluted using a linear gradient from 0 to 100% acetonitrile/water containing 0.1% formic acid over 14 minutes at a 0.3 mL min^{-1} flow rate.

Real-time aggregation kinetics monitoring with turbidity assay

Similar to the ThT fluorescence assay, the synthesized peptides were monomerized with HFIP : TFA (1 : 1) treatment. With a 2.0 mg mL^{-1} concentration of the peptide in filtered BRB80 assay buffer and filtered KCNO (0.2 M) as the polymerizing (carbamylating) agent, the aggregation kinetics was studied for all peptides at 37 °C using a multimode plate reader with the absorbance measured at 400 nm. The process was monitored until the plateau (steady-state phase) absorbance was reached. The experiments were independently repeated three times, and the experimental replicates (triplicate) were averaged, after which the graphs were plotted using GraphPad Prism 9. The error bar represents the standard error.

ANS (8-Anilino-1-naphthalene sulfonic acid) fluorescence assay for amyloidogenicity

The peptide aggregates from the turbidity assay were taken for the ANS fluorescence assay. ANS (8-Anilino-1-naphthalene sulfonic acid) (200 μM) dye was taken with the peptide aggregates in the BRB80 buffer, and the fluorescence was recorded at two time points, initial (t = 0) and post-fibrillization times (t = PF) after incubation at 37 °C in the dark overnight. The excitation and emission wavelengths were 388 nm and 400–600 nm, respectively. The experimental replicates were averaged, and the graph was plotted using GraphPad Prism 9. The error bar represents the standard error.

Circular dichroism of homocitrulline self-assembled peptide amphiphiles

Peptide amphiphile monomers and aggregates of the 5HCT series in water were analyzed using circular dichroism (JASCO J-1500 spectrometer) at 25 °C, and the spectra from 190 nm to 350 nm were obtained. A quartz cuvette of 0.1 cm pathlength with 0.1 mg mL^{-1} concentration of peptides was utilized. The BeStSel webserver tool was used for the analysis of CD data.[41]

Congo-red birefringence fluorescence microscopy of self-assembled peptide amphiphiles

Peptide aggregates were produced, as mentioned previously, without ThT and subjected to ultra-centrifugation at 100 000 RCF at 4 °C to remove salts. The samples were drop-cast onto clean slides, and an alkaline Congo-red dye solution was prepared (80% methanol/20% water containing 1% NaOH), saturated with NaCl, and filtered using a 0.2 μm filter. Microscopic visualization was performed at 50× magnification in polarized and bright field modes (Leica DM4 P Polarization Microscope). The brightness parameters were kept constant for field comparisons. ImageJ was used for birefringence quantification using the manual segmentation method.[42]

Fluorescence microscopy of ThT-bound self-assembled peptide amphiphiles

With inverted fluorescence microscopy, all the peptide amphiphile fibrils (recovered from ThT assay) were taken on glass slides and, with ThT acting as an *in situ* stain, were directly observed at 100× resolution with a FITC filter. An oil immersion technique was employed in the visualization process (Zeiss Axio Observer). The laser power and fluorescence intensity were constant for all samples.

Scanning electron microscopy (SEM) of fibrillar structures formed by peptide amphiphiles

Peptide aggregates from the ThT assay were collected and subjected to ultra-centrifugation at 100 000 RCF at 4 °C to remove salts that interfere with SEM. On clean glass slides, the peptide fibril was drop-cast, dried, and spur-coated for

Peptide series	N-terminus (N)	C-terminus (C)	Resultant polylysine
3K (N-K-K-K-C)	$CH_3C(=O)$-	-$CONH_2$	3KC2
	$CH_3CH_2CH_2CH_2CH_2C(=O)$-		3KC6
	$CH_3CH_2CH_2CH_2CH_2CH_2CH_2CH_2C(=O)$-		3KC9
5K (N-K-K-K-K-K-C)	$CH_3C(=O)$-	-$CONH_2$	5KC2
	$CH_3CH_2CH_2CH_2CH_2C(=O)$-		5KC6
	$CH_3CH_2CH_2CH_2CH_2CH_2CH_2CH_2C(=O)$-		5KC9
8K (N-K-K-K-K-K-K-K-K-C)	$CH_3C(=O)$-	-$CONH_2$	8KC2
	$CH_3CH_2CH_2CH_2CH_2C(=O)$-		8KC6
	$CH_3CH_2CH_2CH_2CH_2CH_2CH_2CH_2C(=O)$-		8KC9

(a)

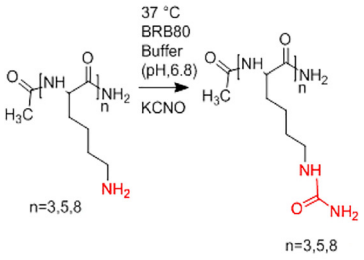

(b)

Fig. 1 (a) Peptide checklist containing nine peptide combinations synthesized by varying peptide lengths (3K, 5K, and 8K) and three N-terminus capping (C2, C6, and C9 carboxylic acids). The peptides were synthesized by Fmoc-SPPS (solid phase peptide synthesis) on rink amide resin. (b) Schematics of carbamylation of polylysine peptide amphiphiles with KCNO as a carbamylating agent.

50 seconds with platinum to prepare the samples for SEM. JEOL FE-SEM captured the images with an acceleration voltage of 5 kV.

Cytotoxicity analysis of homocitrulline peptide amphiphiles using CellTiter-Blue assay

5HCT series monomers and aggregates (concentration of 0.25 mg mL^{-1}) were subjected to cytotoxicity analysis in SH-SY5Y cells with CellTiter-Blue (Promega). The cells were grown with DMEM/F12 (Dulbecco's Modified Eagle Medium/Nutrient Mixture F-12 Ham) media supplemented with 10% FBS (Fetal Bovine Serum). Triplicates of 0.5×10^5 cell seeding density were seeded on 96-well clear flat-bottom plates, as per the manufacturer's instructions. Absorbance measurements at 570 nm and 600 nm (reference) were obtained to help quantify the resorufin produced by viable cells.

Results and discussion

Design and synthesis of peptide amphiphiles (PA)

In a previous study, we demonstrated that carbamylation of lysine residues can convert non-aggregating peptide sequences into readily self-assembling ones and this was used to identify hidden aggregation hotspots in tau protein.[38] We hypothesized that this ''stickiness'' of carbamylated lysines (also referred to as homocitrulline) could be exploited to create well-defined fibrillar nanostructures from homo-oligomers. Furthermore, adding a lipophilic tail can be used to provide an amphiphilic character to these homo-oligomeric sequences and equip us with an excellent handle to further tune the structure and properties by varying the tail length. In addition, the convenience of *in situ* carbamylation to create carbamylated lysine homo-oligomers from easily assembled and water-soluble oligomeric lysines provided us additional flexibility to work across a range of concentrations and play with self-assembly kinetics for fine control over self-assembled nanostructures.

For the current study, we have chosen 3K, 5K and 8K peptides as surrogates for PAs with 3, 5 and 8 carbamylated lysine repeat peptides. As lipophilic tails, we chose hexanoic and nonanoic acids to provide a saturated 6- and 9-carbon-long straight-chain aliphatic appendage. N-terminal acetylated sequences, which effectively add two carbon chains, were used as a control for comparison. 9 PAs were used in the current study (Fig. 1). 5HCT series with five homocitrulline residues containing alkyl tails was also synthesized to highlight the similarities in behaviour and properties. The 5-mer homocitrulline peptides (5HCT series) could be achieved only with microwave-assisted synthesizers; meanwhile, beyond five residues, strong on-resin aggregation was observed, leading to complications in the synthesis and characterization of homocitrulline peptides, and therefore, they have not been included in the study.

In situ carbamylation and self-assembly of PAs: aggregation kinetics studies with ThT fluorescence and turbidity assays

All nine lysine-containing PAs in BRB80 buffer with varying concentrations (2.0, 1.0, 0.50, 0.25, 0.13, 0.06, 0.03 mg mL^{-1}) were exposed to 0.2 M KCNO, which resulted in *in situ* carbamylation of the PAs. This carbamylation of side-chain amine functionality is extremely fast, and two hours is sufficient to effect complete transformation.[43] To monitor the *in situ* self-assembly of carbamylated PAs, thioflavin-T, a benzothiazole reporter dye molecule known to possess selective affinity towards rich β-sheet forming structures,[44] was used. As aggregation proceeds and self-assembled fibrillar structures evolve, they bind to ThT and induce characteristic fluorescence emission at 485 nm. The real-time sigmoidal aggregation curve was visualized from the assay for carbamylated PAs, starting from the lag phase (nucleation), a log phase (elongation) and to steady-state (plateau) phases, demonstrating fibrillar growth for all peptides except 3KC2 (Fig. 2–4). All peptide concentrations showed aggregation with differences in the time of development and arrival of each phase. The lag phase provides information on the time duration for primary and secondary nucleation stages, while the log phase denotes the time and rate of fibrillar growth.[45] The control peptides (identical conditions but without adding KCNO, *i.e.*, no carbamylation) exhibited no ThT fluorescence signal with time, indicating no aggregation in surrogate lysine PAs despite having amphiphilic characteristics.

To confirm if the resulting self-assembled fibrillar nanostructures contained partially or fully carbamylated PAs,

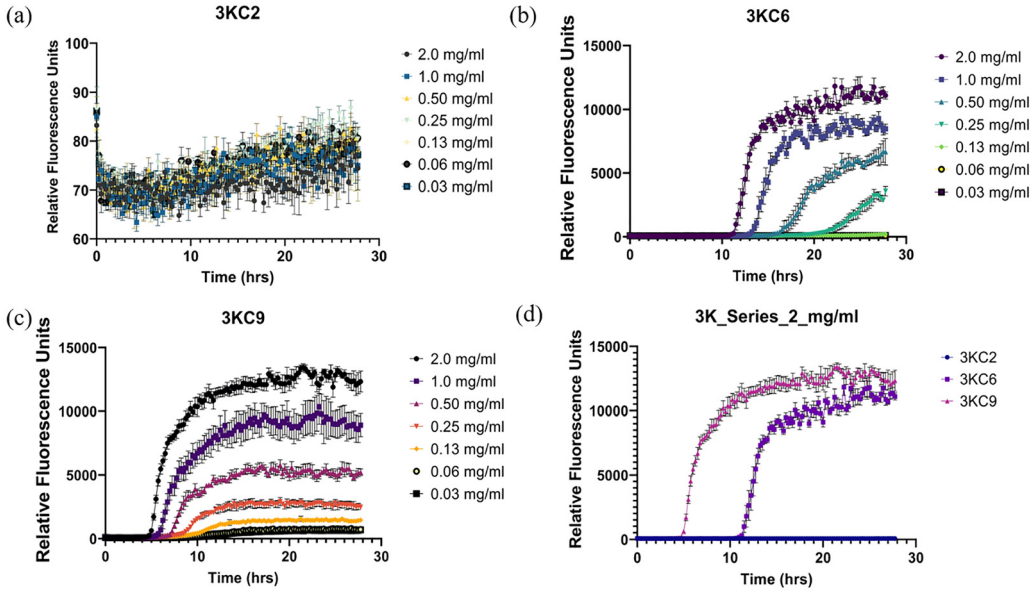

Fig. 2 Real-time aggregation monitored by ThT fluorescence-based aggregation assay for the 3K peptide series at various peptide concentrations. (a) 3KC2, (b) 3KC6, (c) 3KC9, and (d) comparison of the aggregation profiles of all three peptides at 2 mg mL^{-1}. The assay was performed with a BRB80 buffer (pH 6.8) at 37 °C. Error bars indicate standard error.

aggregates were retrieved, melted in TFA to give monomers, and analyzed by LC-MS. The respective masses (m/z) of the peptides before and after *in situ* carbamylation and aggregation can be found in Tables S1 and S2. We could confirm that in all the cases, fibrillar aggregates were entirely composed of PAs with all lysines fully carbamylated.

The aggregation kinetics of carbamylated PAs showed variability based on concentration, number of hydrophilic lysine residues, and length of the hydrophobic alkyl chains. For lower concentrations, the 8K series aggregated quickly than the 5K and 3K series, and the C9-tailed peptides aggregated faster than the C6 or C2 peptides. However, at higher concentrations, these differences disappeared. Generalizing, we could visualize the length of peptides and acyl chains as inversely related to the time of aggregation, with the hydrophobic tail effects overpowering the effects of hydrophilic residues. Eight out of nine peptides (except 3KC2) showed significant amyloidogenicity from this assay. The sigmoidal curves from the ThT assay can

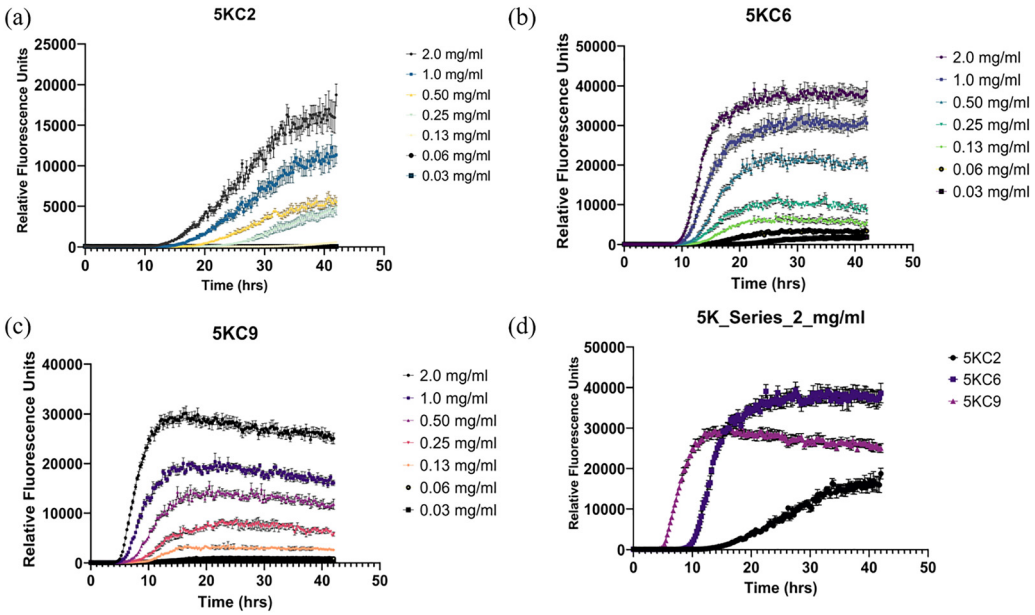

Fig. 3 Real-time aggregation monitored by ThT fluorescence-based aggregation assay for the 5K peptide series at various peptide concentrations. (a) 5KC2, (b) 5KC6, (c) 5KC9 and (d) comparison of the aggregation profiles of all three peptides at 2 mg mL^{-1}. The assay was performed with a BRB80 buffer (pH 6.8) at 37 °C. Error bars indicate standard error.

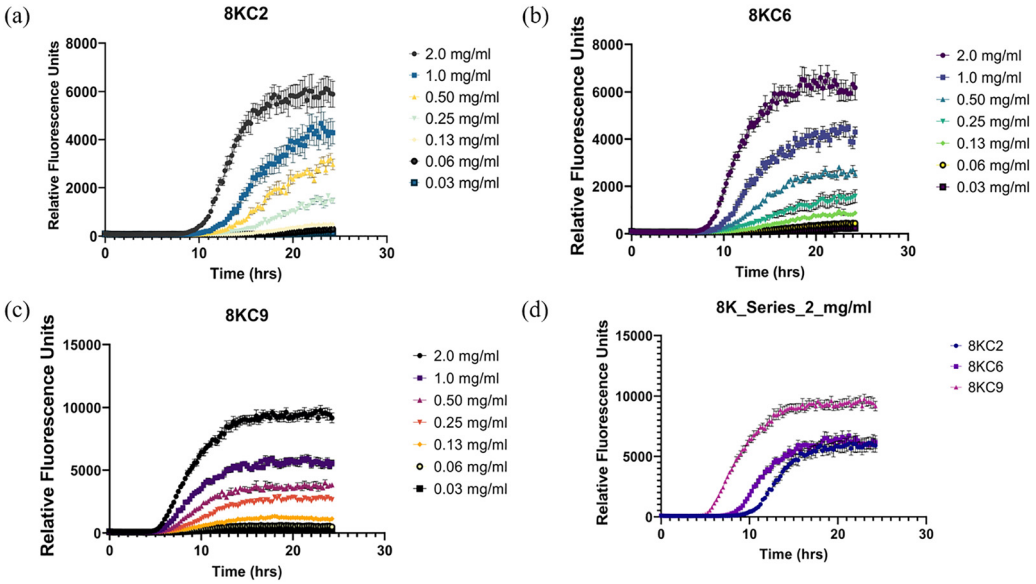

Fig. 4 Real-time aggregation monitored by ThT fluorescence-based aggregation assay for the 8K peptide series at various peptide concentrations. (a) 8KC2, (b) 8KC6, (c) 8KC9, and (d) comparison of the aggregation profiles of all three peptides at 2 mg mL^{-1}. The assay was performed with a BRB80 buffer (pH 6.8) at 37 °C. Error bars indicate standard error.

be found in Fig. 2, 3, and 4, representing the 3K, 5K, and 8K peptide series, respectively, with C2, C6, and C9 N-terminal modifications.

To further understand the aggregation kinetics data across PAs, we selected the ThT assay 2.0 mg mL^{-1} concentration and analyzed the ThT fluorescence data by fitting the sigmoidal curves obtained using the following equation.[46]

$$Y = y_i + m_i t + \frac{y_f + m_f t}{1 + e^{-\left[(t - t_{1/2})/\tau\right]}}$$

here, Y is the fluorescence intensity existing as a function of time t, y_i, and y_f are the intercepts of the initial baseline and plateau intensities with the y-axis (relative fluorescence intensity), and m_i and m_f indicate the respective slopes (both considered zero in our case). $t_{1/2}$ is the time required to reach half the plateau intensity. τ is the elongation time constant calculated by fitting data from five replicates in the above equation and averaged to reduce unintended bias, such as the appearance of a biphasic sigmoidal curve. The growth of all PA fibrils was captured with their respective k_{app}, the apparent rate constant for fibril growth, obtained from $1/\tau$, while the lag time was calculated using $t_{lag} = t_{1/2} - 2\tau$. Table 1 provides $t_{1/2}$, k_{app}, t_{lag}, and maximum plateau ThT intensity values derived from the ThT fluorescence curves of 2.0 mg mL^{-1} concentration. The supplementary section contains calculated kinetic parameters for the other remaining concentrations (Table S3).

Within a series of PAs with the same number of carbamylated lysine residues, $t_{1/2}$ and t_{lag} decreased with increasing tail length from C2 to C9, hinting at a strong dependence of kinetics on lipophilic tail lengths. However, no such trend could be deduced when comparing the variation in the number of carbamylated lysine residues while keeping the tail the same. If we assume that plateau ThT fluorescence represents a measure of amyloidogenicity, the 5K series appears to yield fibrillar PAs with exceedingly high amyloid content.

The critical concentration of fibrillization was determined for the 3K, 5K and 8K series of carbamylated polylysines to check for a pattern across and within the series (Table 2). The maximum observed plateau ThT value was plotted against the

Table 1 ThT fluorescence curve-derived values of $t_{1/2}$, k_{app}, t_{lag}, and maximum plateau ThT intensity for the 3K, 5K, and 8K peptide series at 2.0 mg mL^{-1} concentration

Peptide	$t_{1/2}$ (h)	k_{app} (h^{-1})	t_{lag} (h)	Maximum plateau ThT intensity (A.U.)
3KC2	15.00 ± 0.3	0.73 ± 0.4	17.71 ± 0.6	80.6 ± 4.42
3KC6	12.50 ± 0.3	0.58 ± 0.6	9.08 ± 1.1	12 210.9 ± 279.87
3KC9	5.25 ± 0.4	2.16 ± 1.7	4.82 ± 0.6	14 222.0 ± 813.74
5KC2	31.75 ± 0.2	0.19 ± 0.1	17.01 ± 0.2	19 749.0 ± 1375.57
5KC6	16.75 ± 0.2	0.38 ± 0.5	8.05 ± 0.7	41 648.4 ± 1881.07
5KC9	7.75 ± 0.3	1.39 ± 0.9	6.3 ± 0.4	25 067.4 ± 950.75
8KC2	13.50 ± 0.1	0.74 ± 0.8	10.8 ± 0.1	5889.6 ± 520.80
8KC6	11.50 ± 0.6	0.41 ± 0.7	6.61 ± 0.8	6581.2 ± 499.58
8KC9	8.25 ± 0.5	0.39 ± 0.6	3.21 ± 0.9	9767.4 ± 327.89

Table 2 Critical concentration values calculated for the 3K, 5K and 8K peptide series

Peptide series	Critical concentration (μg mL^{-1})
3KC2	Not determined as no significant difference in aggregation with concentration was observed by ThT kinetics
3KC6	15.9
3KC9	8.5
5KC2	8.2
5KC6	6.5
5KC9	3.4
8KC2	14.9
8KC6	7.5
8KC9	6.6

initial concentration of the peptides to arrive at the critical concentration.

From Table 2, we can observe the decrease in critical concentration values (except 3KC2, which could not be determined), with an increase in tail lengths within a particular series, which is in accordance with ThT kinetics data. Therefore, the effect of hydrophobic alkyl tails in dictating the fibrillogenesis can be visualized clearly. The 5K series tends to aggregate quickly compared to the other series, while also maintaining the trend of faster fibrillization in C9 tails than in C2 tails. The supplementary section contains the regression plots for critical concentration determination (Fig. S9).

The 5HCT series was subjected to the ThT aggregation assay, and the corresponding fluorescence curves are provided in Fig. S8. Although the nature of the curve was sigmoidal and similar to the carbamylated 5K series, some shortening of the lag phase was observed for all three peptides. This was anticipated as the lag time for the original KCNO-induced aggregation kinetics assay of the 5K series that included the time required for the *in situ* carbamylation reaction, which precedes aggregation. The Amylofit tool was utilized to better understand the aggregation mechanism of the 5HCT series.[47] The best fit for the ThT aggregation kinetics data was provided by – saturating elongation and secondary nucleation – unseeded model, which closely represented the aggregation kinetics across these peptides (Fig. S8). By saturating elongation, the model implies that the growing fibrils tend to take up monomers from the solution with the addition of these monomeric units to the ends of the fibrils, hence the term 'elongation'. The saturating elongation can be observed with the significant lag phase in all the 5HCT series peptides across concentrations. The secondary nucleation phenomenon implies that the existing fibrils tend to catalyze the formation of newer nuclei from the monomer pool in the solution. This phenomenon is heavily concentration-dependent, as also seen from our study, where, based on the initial concentration of the monomers, the rate and kinetics of aggregation vary, with higher concentrations showing faster aggregation (Table S4). Consistent with our earlier observations, an increase in the hydrophobic tail length accelerated the aggregation kinetics within each series of peptides with a fixed number of carbamylated lysine residues.

Control polylysine amphiphiles used in the present study did not exhibit any self-assembly, whereas strong fibrillization was observed upon carbamylation. This suggests that electrostatic repulsion among the unmodified, highly polar lysine side chains dominates over the hydrophobic contributions from the lipid tails, thereby preventing self-assembly. Polylysine-based lipopeptides have been widely employed in biomedical applications, with literature reports typically utilizing chains composed of at least 11 or more lysine residues and alkyl chains of carbon length 12 or longer.[48,49] Furthermore, a critical aggregation concentration (CAC) has not been documented for short peptide amphiphiles.[50] Thus, we hypothesize that carbamylation effectively reduces the net charge, enabling even short polylysine amphiphiles to assemble into fibrillar nanostructures upon carbamylation, a property absent in their unmodified counterparts.

Fibrillogenesis in carbamylated polylysine exhibits a non-monotonic dependence on peptide length. For the 3K series, the peptide length may be too short for the formation of stable β-sheet structures. On the other hand, for the 8K series, the peptide length may be sufficiently long to display conformational flexibility and competing intramolecular interactions that may hinder ordered assembly, which is reflected in CAC values higher than expected. Based on our studies, an intermediate length (5K) seems to achieve a balance of structural flexibility and nucleation efficiency, thereby showing the highest propensity for fibril formation. However, to conclusively substantiate these mechanistic interpretations, further high-resolution structural studies, such as cryo-EM, will be required to better define the aggregation landscape in the context of varying lysine and alkyl chain length.

Additionally, a turbidity assay was performed to understand the self-assembly of carbamylated polylysines devoid of ThT to rule out any artifacts arising due to the presence and binding of ThT. The turbidity assay has low sensitivity but is immensely helpful in capturing the evolution of the aggregated material

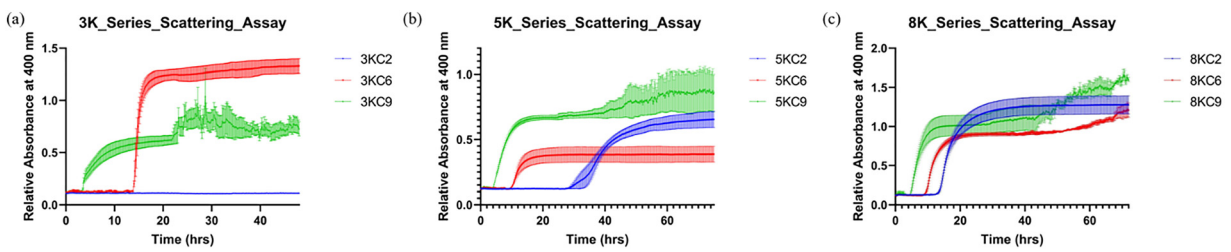

Fig. 5 Turbidimetry test of the 3K, 5K, and 8K peptide series. Light scattering absorbance at 400 nm was measured for the (a) 3K, (b) 5K, and (c) 8K peptide series with varying N-terminal capping C2, C6, and C9 tails. Error bars indicate standard error.

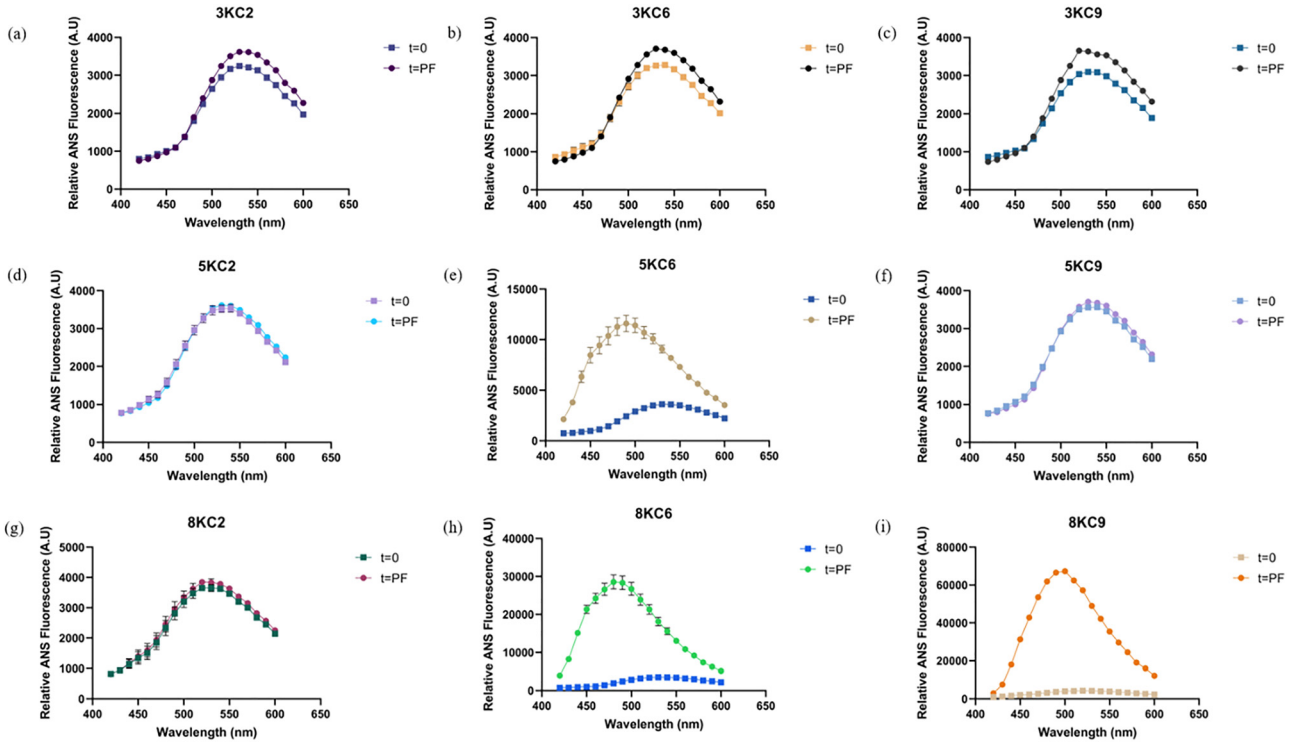

Fig. 6 ANS assay of the 3K, 5K, and 8K peptide series. Relative ANS fluorescence curves measured at t = 0 and t = PF (post-fibrilization) of (a) 3KC2, (b) 3KC6, (c) 3KC9, (d) 5KC2, (e) 5KC6, (f) 5KC9, (g) 8KC2, (h) 8KC6 and (i) 8KC9 peptide amphiphile aggregates. Error bars indicate standard error.

purely from a size perspective. All the peptide aggregates exhibited the sigmoidal growth curve, with growth rates varying significantly, except for 3KC2 (Fig. 5). Similar to the ThT fluorescence assay, the 8K series showed quicker growth and aggregation compared to the 5K and 3K series. Based on the tails, the C9-tailed peptides aggregated faster than the C2 peptides. 3KC2 did not exhibit any aggregation, which was in line with the ThT assay. The kinetic parameters ($t_{1/2}$) and trends were also observed to be in line with the ThT aggregation parameters (Table S5). The $t_{1/2}$ observed within the same peptide series was found to decrease with an increase in hydrophobic tail length, while between series, containing the same tails, no significant trend was observed. Other external factors that might potentially affect the aggregation kinetics in carbamylated polylysines could be temperature, pH, and interacting solvent conditions, which warrant deeper investigation in future studies.[51–53]

Therefore, from the ThT fluorescence and turbidity-based kinetic assays, critical concentration determination, and fitting available different protein aggregation models, we could observe that the aggregation propensity seems to be significantly influenced by the hydrophobic alkyl tails, while the variation in the number of peptide residues carrying the same hydrophobic tail does not provide much difference in the aggregation behaviour during fibrillogenesis.

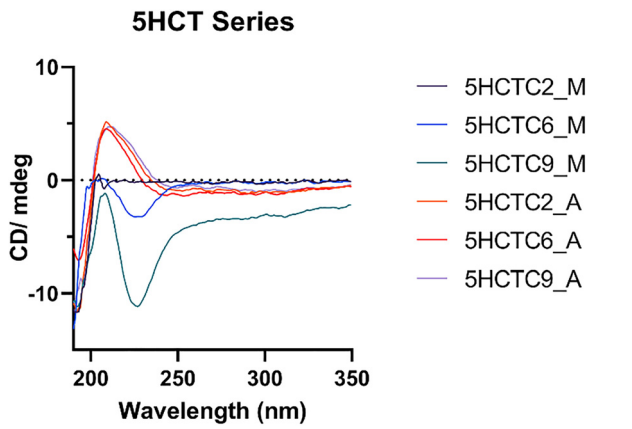

Fig. 7 Circular dichroism of the 5HCT peptide series for monomeric and aggregated samples. The aggregation was carried out at a 2 mg mL^{-1} peptide concentration and diluted to 0.1 mg mL^{-1} for spectroscopic measurements.

Amyloidogenicity of self-assembled carbamylated PAs

An ANS assay was performed to validate the amyloidogenicity of the self-assembled PAs. ANS, a hydrophobic dye, selectively binds to amyloid structures, providing a blue shift in the emission maxima with increased fluorescence intensity.[54] The graphs and ANS fluorescence intensity data can be found in Fig. 6 and Table S3. The blue shift between initial and post-fibrillization reads indicates the amyloidogenic nature of the peptides, thereby confirming the amyloidogenicity of the peptide amphiphiles. No significant blue shift was observed for peptides, except 5KC6, 8KC6, and 8KC9. This deficient performance of the ANS assay and the absence of the correlation of

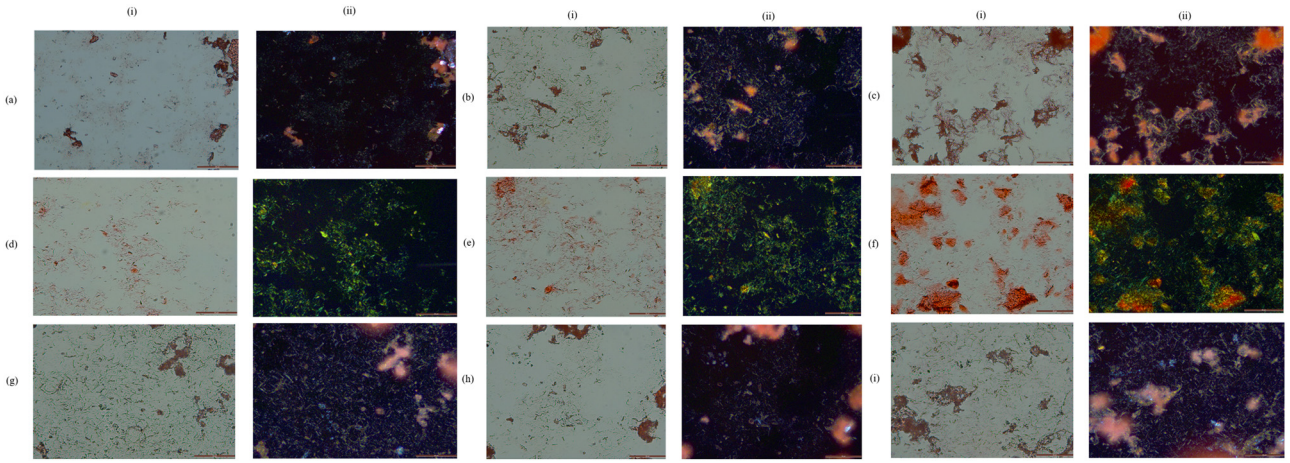

Fig. 8 Representative Congo red dye-based birefringence test microscopy images of (a) 3KC2, (b) 3KC6, (c) 3KC9, (d) 5KC2, (e) 5KC6, (f) 5KC9, (g) 8KC2, (h) 8KC6, and (i) 8KC9 peptide amphiphile aggregate images from (i) bright field and (ii) cross-polarized light views, respectively, at 50× magnification. Apple-green/golden birefringence denotes the presence of amyloidogenic properties. The images correspond to the aggregation reaction with a peptide concentration of 2 mg mL^{-1}. The scale bar corresponds to 50 μm.

results obtained from the ThT assay could be attributed to the absence of hydrophobic patches (other than the tail) in the peptides studied, which may impair the binding of the ANS dye to the self-assembled PA fibrils.

The 3K, 5K and 8K series of carbamylated polylysine amphiphiles could not be analysed with CD due to high salt interference from KCNO. However, to ascertain the presence of the β-sheet structure upon aggregation, CD analysis was performed on both monomers and aggregates (fibrils) of the 5HCT series (Fig. 7). Monomer amphiphiles predominantly exhibited α-helix structures, with the helical content increasing with the length of the alkyl tail. In contrast, the fibrillary aggregates displayed prominent β-sheet structures; in particular, an anti-parallel conformation was observed (Table S7).

As an alternative analysis, we relied on Congo-red dye, which tends to exhibit a characteristic apple-green/golden birefringence upon interaction with amyloid fibrils, and this property is utilized to visualize the amyloidogenicity of peptide amphiphiles and help distinguish them from amorphous aggregates. Eight peptides (except 3KC2) showed strong apple-green/golden

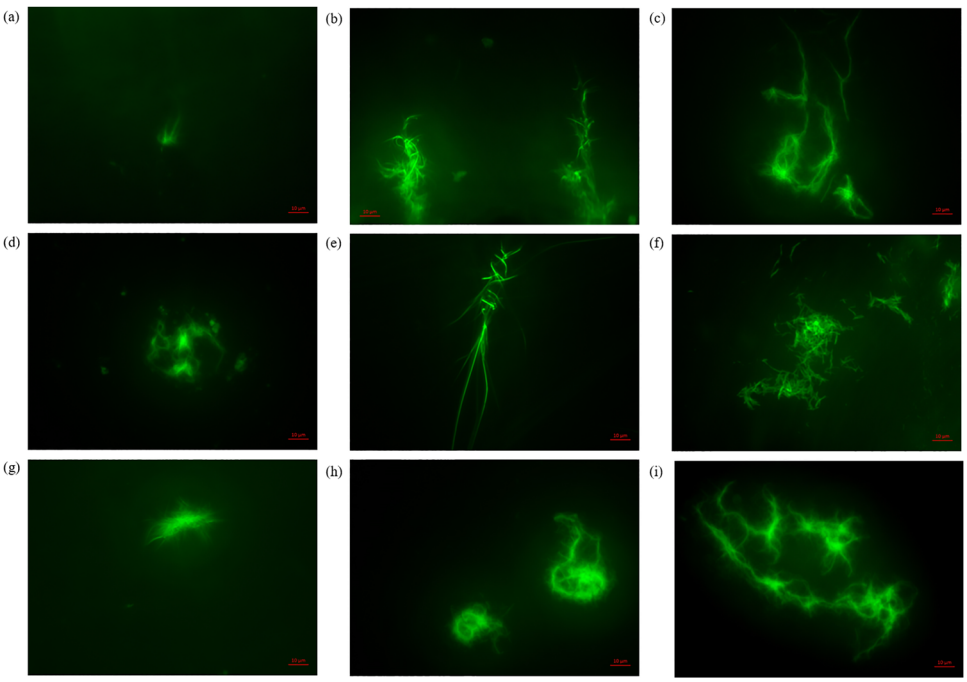

Fig. 9 Fluorescence microscopy of the 3K, 5K, and 8K peptide series. Representative fluorescence microscopy images of (a) 3KC2, (b) 3KC6, (c) 3KC9, (d) 5KC2, (e) 5KC6, (f) 5KC9, (g) 8KC2, (h) 8KC6, and (i) 8KC9 at 100× oil-immersion magnification with the FITC filter. The scale bar corresponds to 10 μm.

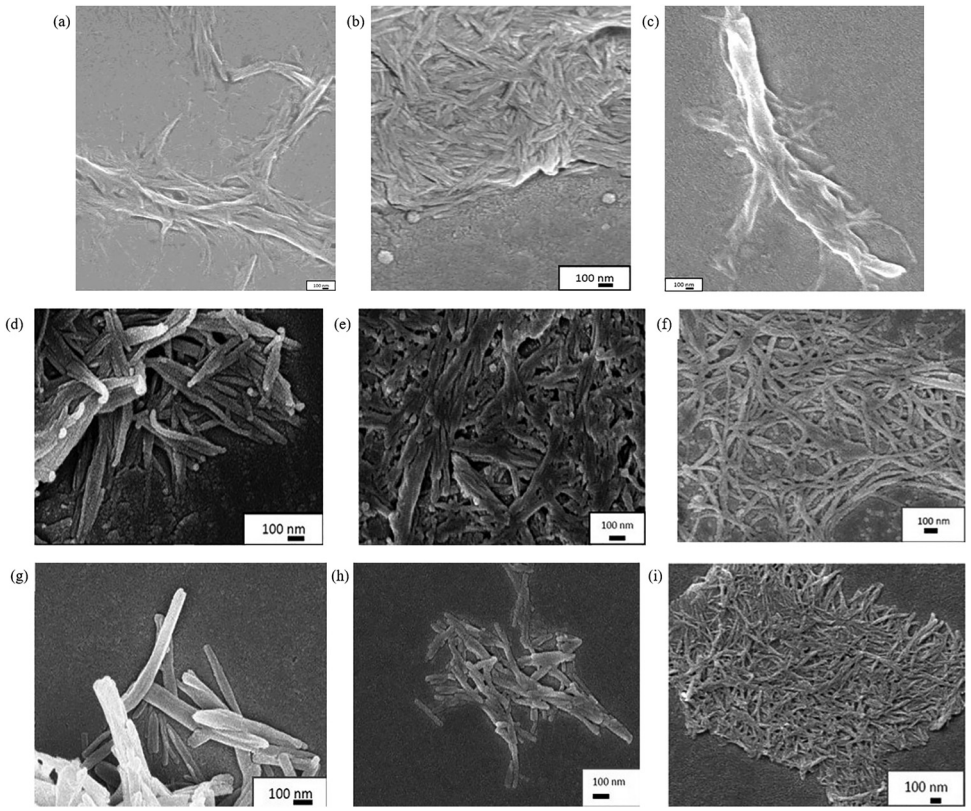

Fig. 10 Representative scanning electron microscopy images (SEM) of (a) 3KC2, (b) 3KC6, (c) 3KC9, (d) 5KC2, (e) 5KC6, (f) 5KC9, (g) 8KC2, (h) 8KC6, and (i) 8KC9 peptide amphiphile aggregates. SEM images were acquired after allowing them to aggregate at 37 °C in the BRB80 aggregation buffer, and post-subjecting to ultra-centrifugation to ensure the absence of salts. The samples were prepared fresh on clean glass slides, platinum spur-coated and transferred to the grid for imaging. The scale bar corresponds to 100 nm.

birefringence, indicating their amyloidogenicity (Fig. 8). The 5K series exhibited particularly prominent levels of birefringence that correlated with high ThT fluorescence levels observed in the ThT assay. The quantification of birefringence across the 3K, 5K and 8K series was performed using the ImageJ tool with a manual segmentation method, and the quantification data can be found in the supplementary section (Fig. S11).[42]

Therefore, from the ANS assay, circular dichroism analysis and Congo-red birefringence, we could visualize the rich beta-sheet formation occurring in the carbamylated polylysine peptide amphiphiles of the 5K series with varying hydrophobic tails, which show significant amyloidogenicity in comparison to the 3K and 8K series.

Fibrillar morphology of self-assembled PAs

Using ThT *in situ* fluorescence, the aggregates were visualized with a fluorescence microscope using a FITC filter, revealing the fibrillar forms/thread-like structures across all nine peptides of variable lengths. Thick tufts of peptide fibrils with high fluorescence intensity could be observed, highlighting the propensity of these carbamylated polylysine peptide amphiphiles to form fibrils exhibiting amyloidogenicity. The 3K series peptides showed shorter, less dense, atypical hair-like strands of fibrils, while the 5K and 8K series showed dense fibrils. 3KC2 had little to no fibrils, while all the other eight peptides exhibited a dense fibrillar arrangement. The representative images of the 3K, 5K, and 8K peptide series, respectively, with C2, C6, and C9 N-terminal modifications, can be found in Fig. 9.

The verification of fibrillar structures formed by peptide amphiphiles was performed using SEM to look for significant morphological features across the peptides. All the observed fibrils exhibited a mesh-like arrangement with twisted thread-like peptides interwoven across layers. The SEM images of the 3K, 5K, and 8K series peptides can be found in Fig. 10. The average thickness (n = 10) of these fibrils formed is listed in Table 3.

The 3K peptide series had finer fibrils, as opposed to the 5K and 8K series, which seemed much thicker. 8KC9 was the

Table 3 Fibril thickness of the 3K, 5K, and 8K peptide series measured post-SEM imaging (n = 10)

Peptide	Thickness of fibrils (mean ± SD) (nm)
3KC2	8.2 ± 0.5
3KC6	29.0 ± 0.7
3KC9	46.4 ± 0.8
5KC2	18.8 ± 0.8
5KC6	41.2 ± 0.5
5KC9	56.9 ± 0.8
8KC2	24.0 ± 0.5
8KC6	47.5 ± 0.9
8KC9	68.9 ± 0.4

densest of all peptide fibrils, indicating a direct relationship between the fibril thickness and the length of the peptide chain/its N-terminus modification.

From the microscopic visualization of polylysines, a thick mesh-type arrangement could be observed, strikingly close to those reported in antimicrobial peptides containing lysine–phenylalanine residues exhibiting rigid-rod-like structures.[55] Similarly, in tyrosine–lysine peptides, variation in the position and number of lysine residues was shown to affect the monomer and aggregate nature, eventually affecting the structure.[56] This phenomenon could be observed in carbamylated polylysines as the charge neutralization of lysines is considered a key event for these species to exhibit self-assembly and fibrillogenesis. Lysine-containing peptides, in general, have been shown to exhibit stiff interfaces with differential curvature and packing, arranging themselves in a range of morphologies from spherical micelles, worm-like micelles, and compact vesicles, with alterations when changes in pH and temperature are introduced.[57] Recombinant silk rich in polylysines is also known to be modulated into producing cell-binding peptides and targeting.[58] In Huntingtin amphipathic structures, lysine residues have been found to be essential in fibrillar aggregate seeding, while islet amyloid polypeptides also highlight the importance of lysine residues and their mutations in the progression of the aggregation process, at times affecting the effect of inhibitory drugs for amyloidosis treatment due to their structural properties.[59,60]

In our previous study, carbamylation of PHF6 tau peptide was shown to guide the slow conformational rearrangement of peptides to form ThT-positive amyloid structures, which could be attributed to the structural changes induced by the charge neutralization of lysine residues upon carbamylation.[43] In a follow-up study, we employed this approach to identify hidden aggregation hotspots in the form of lysine-rich short peptide stretches in the tau protein that aggregates when carbamylated.[38] In both studies, peptides were not derivatized with the long alkyl chain, and the fibrillization could be primarily attributed to the charge neutralization of lysine residues, which are modulated by the neighboring residues. By introducing N-terminal alkyl chains of different lengths, this study adds a tunable design element to modulate the self-assembling behavior of carbamylated polylysine amphiphiles.

Cytotoxicity analysis of self-assembled PAs

Cytotoxicity analysis was performed to indicate the biocompatibility of aggregated peptide amphiphiles. Again, the 5HCT series was chosen as the *in vitro* aggregation reactions of the carbamylated 5K series containing KCNO in the reaction pool. A cell viability assay with CellTiter-Blue indicated no significant cytotoxicity to mammalian cells with either 5HCT monomers or aggregates except for the aggregated 5HCTC2 (Fig. 11).

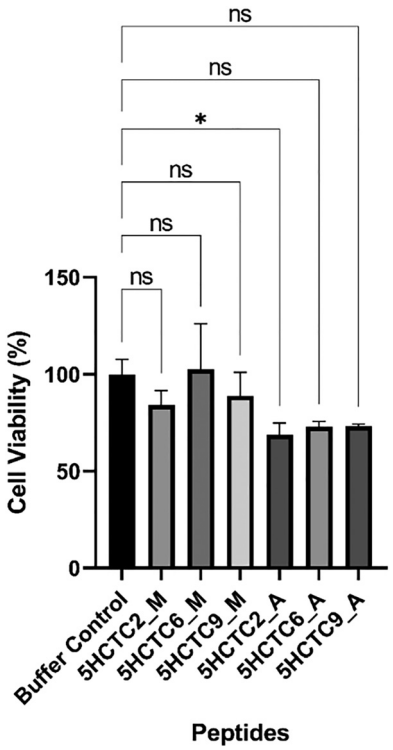

Fig. 11 Cytotoxicity analysis using CellTiter-Blue in the 5HCT peptide series containing both monomeric and aggregate samples. They were subjected to a cell viability assay in SH-SY5Y cells at a concentration of 0.25 mg mL^{-1}.

Conclusion

Our results demonstrated amyloidogenicity in carbamylated lysine repeat peptide amphiphiles and the significance of the number of lysine residues available for carbamylation, along with the influence of hydrophobic tail lengths on modifying aggregation propensity and kinetics. The carbamylation reaction on polylysines is shown to play a vital role in influencing the fibrillar architecture. The amyloidogenicity property of peptide amphiphiles can be harnessed to prepare nanostructures that are highly biocompatible and tunable to achieve the necessary targeted action, thereby opening a new world of possibilities in the field of precision medicine and targeted therapy. Our preliminary results on developing nanostructures with similar self-assembling peptide amphiphiles are promising. Self-assembling peptide amphiphiles could, therefore, be utilized for several broad applications, ranging from drug delivery tools in biomedical nanotechnology to dye degradation applications to curbing pollutant levels in aquatic bodies by industrial discharge, leading to endless possibilities in their functionality due to their limitless potential.

Author contributions

SG and JG conceptualized the study; VS, TP, and JG designed and carried out the experiments. Results were analyzed and the manuscript was written by VS and SG.

Conflicts of interest

There are no conflicts to declare.

Data availability

The data supporting this article have been included as a part of the supplementary information (SI). Supplementary information is available. See DOI: https://doi.org/10.1039/d4ma01239a.

Acknowledgements

The authors thank SERB, Government of India (CRG/2018/004960), for the funding. VS and TP thank MHRD for the fellowship. JG acknowledges the DBT-JRF fellowship. Authors thank the BASyL (Biology of Amyloid Systems Laboratory) & PEPr (Peptide Engineering and Proteomics Research Facility), SMSE (Soft Matter Science and Engineering) laboratory, the Department of Earth Sciences and the Department of Biological Sciences and Engineering, IITGN, for assistance with optical imaging. Support from the Central Instrumentation Facility, IIT Gandhinagar, for SEM is deeply acknowledged.

References

1 S. E. Paramonov, H. W. Jun and J. D. Hartgerink, *J. Am. Chem. Soc.*, 2006, **128**, 7291–7298.
2 J. I. Yeh, S. Du, A. Tortajada, J. Paulo and S. Zhang, *Biochemistry*, 2005, **44**, 16912–16919.
3 D. B. Amabilino, D. K. Smith and J. W. Steed, *Chem. Soc. Rev.*, 2017, DOI: 10.1039/c7cs00163k.
4 E. R. Draper and D. J. Adams, *Chem*, 2017, DOI: 10.1016/j.chempr.2017.07.012.
5 N. E. Ziółkowska, R. Christiano and T. C. Walther, *Trends Cell Biol.*, 2012, DOI: 10.1016/j.tcb.2011.12.002.
6 Y. Zhou, T. Fyrner, C. H. Chen, N. A. Sather, E. L. Hsu, S. I. Stupp and M. L. Snead, *Acta Biomater.*, 2023, **164**, 377–386.
7 W. C. Fowler, *Biomacromolecules*, 2022, **23**, 4804–4813.
8 J. D. Smith, L. N. Cardwell, D. Porciani, J. A. Nguyen, R. Zhang, F. Gallazzi, R. R. Tata, D. H. Burke, M. A. Daniels and B. D. Ulery, *Phys. Biol.*, 2018, DOI: 10.1088/1478-3975/aadb68.
9 V. Castelletto, A. Kaur, R. M. Kowalczyk, I. W. Hamley, M. Reza and J. Ruokolainen, *Biomacromolecules*, 2017, **18**, 2013–2023.
10 N. Nandi, K. Gayen, S. Ghosh, D. Bhunia, S. Kirkham, S. K. Sen, S. Ghosh, I. W. Hamley and A. Banerjee, *Biomacromolecules*, 2017, **18**, 3621–3629.
11 M. H. Sangji, H. Sai, S. M. Chin, S. R. Lee, I. R. Sasselli, L. C. Palmer and S. I. Stupp, *Nano Lett.*, 2021, **21**, 6146–6155.
12 J. A. Hutchinson, I. W. Hamley, J. Torras, C. Alemán, J. Seitsonen and J. Ruokolainen, *J. Phys. Chem. B*, 2019, **123**, 614–621.
13 S. G. Marapureddy, P. Hivare, A. Sharma, J. Chakraborty, S. Ghosh, S. Gupta and P. Thareja, *Carbohydr. Polym.*, 2021, DOI: 10.1016/j.carbpol.2021.118254.
14 N. A. Mansukhani, E. B. Peters, M. M. So, M. S. Albaghdadi, Z. Wang, M. R. Karver, T. D. Clemons, J. P. Laux, N. D. Tsihlis, S. I. Stupp and M. R. Kibbe, *Macromol. Biosci.*, 2019, DOI: 10.1002/mabi.201900066.
15 J. C. Barrett and M. V. Tirrell, in *Methods in Molecular Biology*, Humana Press Inc., 2018, vol. 1798, pp. 277–292.
16 J. Chen and X. Zou, *Bioact. Mater.*, 2019, DOI: 10.1016/j.bioactmat.2019.01.002.
17 M. J. Webber, C. J. Newcomb, R. Bitton and S. I. Stupp, *Soft Matter*, 2011, **7**, 9665–9672.
18 R. J. Williams, A. M. Smith, R. Collins, N. Hodson, A. K. Das and R. V. Ulijn, *Nat. Nanotechnol.*, 2009, **4**, 19–24.
19 A. M. Kloxin, A. M. Kasko, C. N. Salinas and K. S. Anseth, *Science*, 1979, **2009**(324), 59–63.
20 J. B. Matson and S. I. Stupp, *Chem. Commun.*, 2012, **48**, 26–33.
21 C. Xie, Y. Chen, L. Wang, K. Liao, B. Xue, Y. Han, L. Li and Q. Jiang, *Bioact. Mater.*, 2024, DOI: 10.1016/j.bioactmat.2024.06.013.
22 M. Amit, S. Yuran, E. Gazit, M. Reches and N. Ashkenasy, *Adv. Mater.*, 2018, DOI: 10.1002/adma.201707083.
23 L. W. Chow, R. Bitton, M. J. Webber, D. Carvajal, K. R. Shull, A. K. Sharma and S. I. Stupp, *Biomaterials*, 2011, **32**, 1574–1582.
24 K. M. Galler, L. Aulisa, K. R. Regan, R. N. D'Souza and J. D. Hartgerink, *J. Am. Chem. Soc.*, 2010, **132**, 3217–3223.
25 S. Al-Halifa, M. Babych, X. Zottig, D. Archambault and S. Bourgault, *Pept. Sci.*, 2019, DOI: 10.1002/pep2.24095.
26 I. W. Hamley, *Angew. Chem., Int. Ed.*, 2007, DOI: 10.1002/anie.200700861.
27 Y. Yu, X. Jiang, S. Gong, L. Feng, Y. Zhong and Z. Pang, *Nanoscale*, 2014, **6**, 3250–3258.
28 H. Cui, M. J. Webber and S. I. Stupp, *Biopolymers*, 2010, DOI: 10.1002/bip.21328.
29 G. R. Stark, *Reactions of Cyanate with Functional Groups of Proteins. III. Reactions with Amino and Carboxyl Groups*, UTC, 1949, vol. 22.
30 G. R. Stark, Reactions of Cyanate with Functional Groups of Proteins. II. Formation, Decomposition, and Properties of iV-Carbamylimidazole* The abbreviations used are: IMH+ and IM for protonated and unprotonated imidazole, IMCONH2 and IMH + CONHs for unprotonated and protonated N-carbamylimidazole, *Biochemistry*, 1965, DOI: 10.1021/bi00879a032.
31 G. R. Stark, *Reactions of Cyanate with Functional Groups of Proteins. IV. Inertness of Aliphatic Hydroxyl Groups. Formation of Carbamyl-and Acylhydantoins*, UTC, 2024, vol. 11.
32 D. G. Smyth, Carbamylation of amino and tyrosine hydroxyl groups preparation of ajs inhibitor of oxytocin with no intrinsic activity on the jsolated uterus, 1967, vol. 242.
33 M. Holzer, M. Gauster, T. Pfeifer, C. Wadsack, G. Fauler, P. Stiegler, H. Koefeler, E. Beubler, R. Schuligoi, A. Heinemann and G. Marsche, *Antioxid. Redox Signaling*, 2011, **14**, 2337–2346.
34 D. El-Gamal, S. P. Rao, M. Holzer, S. Hallström, J. Haybaeck, M. Gauster, C. Wadsack, A. Kozina, S. Frank, R. Schicho, R. Schuligoi, A. Heinemann and G. Marsche, *Kidney Int.*, 2014, **86**, 923–931.

35 Z. Wang, S. J. Nicholls, E. R. Rodriguez, O. Kummu, S. Hörkkö, J. Barnard, W. F. Reynolds, E. J. Topol, J. A. DiDonato and S. L. Hazen, *Nat. Med.*, 2007, **13**, 1176–1184.
36 M. T. Velasquez, A. Ramezani and D. S. Raj, *Kidney Int.*, 2015, DOI: **10.1038/ki.2015.78**.
37 K. Bhavsar, V. Shekhar and S. Gupta, *Indian J. Biochem.*, 2023, DOI: **10.56042/ijbb.v60i9.4103**.
38 J. Gadhavi, S. Shah, T. Sinha, A. Jain and S. Gupta, *FEBS J.*, 2022, **289**, 2562–2577.
39 X. Zhao, G. S. Liu, Y. Liu, J. Wang, K. Satkunendrarajah and M. Fehlings, The role of neural precursor cells and self assembling peptides in nerve regeneration, 2013, DOI: **10.1186/1916-0216-42-6**.
40 K. Ralhan, V. G. KrishnaKumar and S. Gupta, *RSC Adv.*, 2015, **5**, 104417.
41 A. Micsonai, F. Wien, É. Bulyáki, J. Kun, É. Moussong, Y. H. Lee, Y. Goto, M. Réfrégiers and J. Kardos, *Nucleic Acids Res.*, 2018, **46**, W315–W322.
42 L. L. Smith, A. H. Beggs and V. A. Gupta, *J. Visualized Exp.*, 2013, DOI: **10.3791/50925**.
43 V. Guru KrishnaKumar, L. Baweja, K. Ralhan and S. Gupta, *Biochim. Biophys. Acta, Gen. Subj.*, 2018, **1862**, 2590–2604.
44 C. Xue, T. Y. Lin, D. Chang and Z. Guo, *R. Soc. Open Sci.*, 2017, DOI: **10.1098/rsos.160696**.
45 S. K. Shoffner and S. Schnell, *Phys. Chem. Chem. Phys.*, 2016, **18**, 21259–21268.
46 K. Gade Malmos, L. M. Blancas-Mejia, B. Weber, J. Buchner, M. Ramirez-Alvarado, H. Naiki and D. Otzen, *Amyloid*, 2017, DOI: **10.1080/13506129.2017.1304905**.
47 G. Meisl, J. B. Kirkegaard, P. Arosio, T. C. T. Michaels, M. Vendruscolo, C. M. Dobson, S. Linse and T. P. J. Knowles, *Nat. Protoc.*, 2016, **11**, 252–272.
48 P. Wan, Y. Wang, W. Guo, Z. Song, S. Zhang, H. Wu, W. Yan, M. Deng and C. Xiao, *ACS Biomater. Sci. Eng.*, 2022, **8**, 903–911.
49 M. Zheng, M. Pan, W. Zhang, H. Lin, S. Wu, C. Lu, S. Tang, D. Liu and J. Cai, *Bioact. Mater.*, 2021, DOI: **10.1016/j.bioactmat.2020.12.001**.
50 X. Yi, P. Wan, W. Shen, X. Zhang, P. Zhang and C. Xiao, *Biomater. Sci.*, 2023, **11**, 6611–6618.
51 J. E. Goldberger, E. J. Berns, R. Bitton, C. J. Newcomb and S. I. Stupp, *Angew. Chem., Int. Ed.*, 2011, **50**, 6292–6295.
52 J. Cui, A. Liu, Y. Guan, J. Zheng, Z. Shen and X. Wan, *Langmuir*, 2010, **26**, 3615–3622.
53 M. R. Tiné, M. Alderighi, C. Duce, L. Ghezzi and R. Solaro, *J. Therm. Anal. Calorim.*, 2011, **103**, 75–80.
54 O. K. Gasymov and B. J. Glasgow, ANS Fluorescence: Potential to Augment the Identification of the External Binding Sites of Proteins, *Biochim. Biophys. Acta*, 2007.
55 N. Özbek, E. L. Vilarrocha, B. V. Jover, E. F. Ventura and B. Escuder, *RSC Adv.*, 2024, **14**, 15120–15128.
56 B. Sun, A. D. Ariawan, H. Warren, S. C. Goodchild, M. In Het Panhuis, L. M. Ittner and A. D. Martin, *J. Mater. Chem. B*, 2020, **8**, 3104–3112.
57 S. Manouchehri, P. Zarrintaj, M. R. Saeb and J. D. Ramsey, *Mol. Pharmaceutics*, 2021, DOI: **10.1021/acs.molpharmaceut.1c00474**.
58 N. C. Abascal and L. Regan, *Open Biol.*, 2018, DOI: **10.1098/rsob.180113**.
59 M. H. Wu, A. C. Chan and L. H. Tu, *Biochimie*, 2020, **177**, 153–163.
60 J. R. Arndt, R. J. Brown, K. A. Burke, J. Legleiter and S. J. Valentine, *J. Mass Spectrom.*, 2015, **50**, 117–126.